Discrete versus 1D Compounds based on Pentagonal Bipyramid Coordination Geometries: A Matter of Solubility?

Céline Pichon, Carine Duhayon, Emilie Delahaye, J. P. Sutter

To cite this version:

Céline Pichon, Carine Duhayon, Emilie Delahaye, J. P. Sutter. Discrete versus 1D Compounds based on Pentagonal Bipyramid Coordination Geometries: A Matter of Solubility?. European Journal of Inorganic Chemistry, 2021, 2021 (48), pp.5112-5118. 10.1002/ejic.202100834 . hal-03510193

HAL Id: hal-03510193

https://hal.science/hal-03510193v1

Submitted on 9 Feb 2022

Discrete *versus* 1D compounds based on pentagonal bipyramid coordination geometries: a matter of solubility?

Céline Pichon,*[,a] Carine Duhayon,[a] Emilie Delahaye,[a] Jean-Pascal Sutter*[,a]

[a] Laboratoire de Chimie de Coordination du CNRS (LCC-CNRS), Université de Toulouse, CNRS, UPS, F-31077 Toulouse, France.

TABLE OF CONTENTS

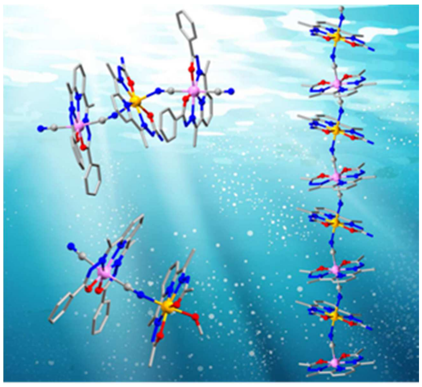

A series of heterometallic compounds based on the association of heptacoordinated *trans*-dicyanido Cr(III) complex $[Cr(L)(CN)_2]K$ and divalent $[Mn^{II}(H_2L^n)Cl_2]$ complexes incorporating pentadentate ligands with a planar N_3O_2 coordination pocket and various R substituents illustrate the subtle effect of R on the selective crystallization of discrete or 1-D heterometallic cyanido-bridged compounds.

Keywords: Chain compounds; Cyanidometallates; Heterometallic complexes; Heptacoordination; Magnetic properties.

Abstract. A series of heterometallic compounds based on the association of *trans*-dicyanido Cr(III) complex $[Cr(L)(CN)_2]K\cdot 2H_2O$ and several divalent $[Mn^{II}(H_2L^n)Cl_2]$ heptacoordinated complexes, where H_2L^n stands for pentadentate ligands featuring a planar N_3O_2 coordination pocket and various substituents (NH_2, cyclohexyl, *S*,*S*-mandelic), is described. A dinuclear compound $[Cr(L)(CN)_2M(H_2L^2)]$ and 1D coordination polymers of general formula $[Cr(L)(CN)_2M(H_2L^n)]X$ ($X = PF_6^-$ or $[Cr(L)(CN)_2]^-$) were rationally prepared by a simple adjustment of the Cr:M stoichiometry for R = NH_2 or tuning the solvent mixtures to promote the crystallization of discrete complexes or chains. The crystal structures, phase purities and magnetic properties of all the compounds are reported.

INTRODUCTION

The building-block approach is an efficient strategy for the synthesis of molecular magnetic materials with specific properties.[1] The versatility of coordination complexes combined to a careful choice of building blocks allows to tune the dimensionality (from discrete to 3-D), the exchange interactions, and provides the possibility to implement additional properties such as optic, photosensitivity, porosity to the magnetic material.[2]

This approach was applied to heptacoordinated complexes with pentagonal bipyramid coordination geometry selected for their substantial magnetic anisotropy with axial Zero-Field Splitting (ZFS) D parameter ranging between -20 and 40 cm^{-1} depending of the electronic configuration of the 3d metal ion.[3] Lanthanide complexes in this surrounding, especially the Dy(III) derivatives, exhibit stronger axial magnetic anisotropies leading to Single-Molecule Magnet (SMM) properties with very high energy barriers up to 1815 K.[4] These complexes exhibit structural robustness of the coordination sphere due to pentadentate ligands stabilizing the equatorial plan making them good building blocks.[5] Recent examples of low-dimensional heterometallic systems (discrete or coordination polymers) made up with $[Cr(L)(CN)_2]^-$ and heptacoordinated Mn(II),[6] Fe(II)[7] and Ni(II)[8] complexes illustrated this approach. The Ising-type magnetic anisotropy ($D < 0$) for Fe(II) and Ni(II) derivatives and their ferromagnetic interactions with Cr(III) units resulted in SMMs and SCMs behaviors.[7,8]

Associations of $[Cr(L)(CN)_2]^-$ with $[Fe(H_2L^1)Cl_2]$ (Scheme 1) evidenced the importance of stoichiometry to isolate either the discrete trinuclear $[Cr_2Fe]$ or the [CrFe] chain.[7a] A series of trinuclear compounds of general formula $[\{Cr(L)(CN)_2\}_2M(H_2L^{N3O2R})]$ (M = Mn and Fe, R = NH_2, cyclohexyl, mandelic) was also obtained in water or H_2O/MeOH mixtures with 2 equivalents of chromium complex *vs.* the divalent entity.[7b] Based on this observation, we were interested to understand the conditions promoting formation (*i.e.* propagation of oligomeric species) and crystallization of chains. Our approach was to study the influence of the peripheral groups R of the pentadentate ligands H_2L^{N3O2R} on the species solubilities. Indeed, it is crucial to control the crystallization of heterometallic species (discrete or 1D) in order to obtain pure samples. Mn(II) complexes with NH_2, cyclohexyl and mandelic substituents (Scheme 1) have been selected to check the effect of steric hindrance and intermolecular interactions on the heterometallic associations. Their syntheses, crystal structures, and magnetic behaviors are described herein.

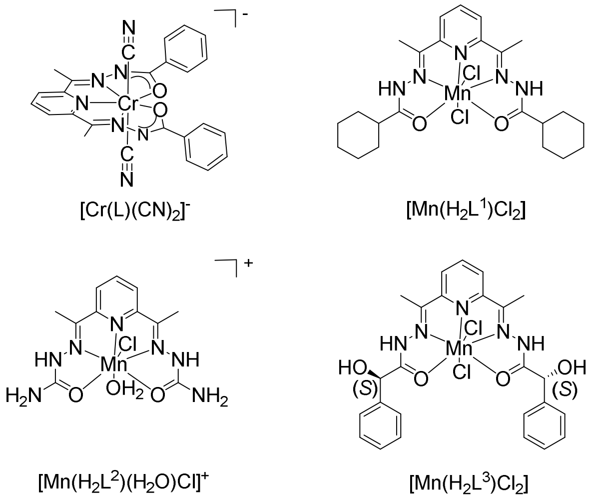

Dinuclear complexes [CrM]:
$[\{Cr(L)(CN)_2\}_2Mn(H_2L^1)(MeOH)](PF_6)$: **1**

Chains [CrM]
$[\{Cr(L)(CN)_2Mn(H_2L^2)](PF_6)$: **2**
$[\{Cr(L)(CN)_2Mn(H_2L^2)][Cr(L)(CN)_2]$: **3**
$[\{Cr(L)(CN)_2Mn(H_2L^3)][Cr(L)(CN)_2]$: **4**

Scheme 1: Sketch of the heptacoordinated metal complexes and heterometallic systems along with their numbering.

RESULTS AND DISCUSSION.

Syntheses.

Associations between $[Cr(L)(CN)_2]^-$ and $[Mn(L^n)Cl_2]$ complexes shown on Scheme 1 were performed with various Cr/Mn ratio by interdiffusion of Mn(II) and Cr(III) solutions in different solvents with the goal to crystallize heterometallic chains. In the case of L^1, crystallization in concentrated methanol medium was fast (one hour) affording the dinuclear complex $[Cr(L)(CN)_2Mn(H_2L^1)(MeOH)](PF_6)\cdot H_2O\cdot 2MeOH$ (**1**). It was not possible to identify the chain $[Cr(L)(CN)_2Mn(H_2L^1)]^+$ even working with a default of $[Cr(L)(CN)_2]^-$. With the ligand H_2L^2, the chain $[Cr(L)(CN)_2Mn(H_2L^2)](PF_6)\cdot 2H_2O\cdot MeOH$ (**2,** ratio Cr/Mn 1:1) was achieved in a 50:50 water/methanol medium whereas a similar chain $[Cr(L)(CN)_2Mn(H_2L^2)][Cr(L)(CN)_2]\cdot 5.5H_2O\cdot 3MeOH$ (**3**) but with one Cr(III) complex as anion was preferentially crystallized in the absence of PF_6^- anions.

In the case of H_2L^3, the nature of the solvent modified the species crystallized. In H_2O/MeOH 50:50, a cationic chain with one chromium as anion, $[Cr(L)(CN)_2Mn(H_2L^3)][Cr(L)(CN)_2]\cdot 6H_2O$ (**4**), was the main product with traces of the trinuclear species even when working with a stoechiometry 1:1. The trinuclear

$[\{Cr(L)(CN)_2\}_2Mn(H_2L^3)]\cdot 13H_2O$[7b] described in a previous work has been crystallized with two equivalents of Cr(III) complex in water.

Solid state infrared spectra for the heterometallic complexes showed a noticeable shift of the cyanide bands towards larger wavenumbers compared to 2130 cm^{-1} for $[Cr(L)(CN)_2]K$.[5] Characteristic bands were found at 2127 and 2150 cm^{-1} for **1**, 2148 and 2153 cm^{-1} for **2,** 2151 and 2160 cm^{-1} for **3** and 2133 and 2161 cm^{-1} for **4**. We can notice that the shift between the two cyanide bands is more pronounced in **1** which can be explained by one terminal and one bridging CN group in this complex whereas the others systems have both bridging Cr(III) units linked by both cyanides.[5,6] Finally, PF_6^- anions were detected in **1** and **2** with strong bands around 845 cm^{-1}.

Crystal structures.

All the compounds have been crystallized and their crystal structures have been solved. General crystallographic data are gathered in Table 1. The metal-ligand bond distances and angles are similar to that found in the starting materials,[9] further details can be found in the Experimental section with selected bond distances and angles. In all the heterometallic compounds, the metal centers are heptacoordinated with a coordination polyhedron close to bipyramid pentagonal geometry (PBP, Table S1). The actual deformations of the PBP coordination geometries have been analyzed by Continuous Shape Measures[10] performed with SHAPE[11] (Table S1). The metal sites are connected through cyanide bridges and the compounds are cationic chains differing by peripheric groups and/or anions except the complex $[Cr(L)(CN)_2Mn(H_2L^1)(MeOH)](PF_6)\cdot H_2O\cdot 2MeOH$ (**1**) which is a discrete complex. **1** is a dinuclear species with one cyanide of the chromium complex connecting the two metallic centers while the second one is terminal (Figure 1). The molecule is slightly bent due to a Mn–N≡C angle of 160.4°. For the Mn(II) atom, a methanol molecule is coordinated in axial position in *trans vs.* the nitrogen atom of the CN bridge (Mn–N = 2.210 Å). However, the organization of the dinuclear entities in the crystal packing is close to chains of dinuclears propagating along the *c* axis through short hydrogen bonds occurring between terminal nitrogen of the free cyanide and the H atom of the methanol coordinated to a neighbouring dinuclear (N···C = 2.75 Å, Figure S1b).

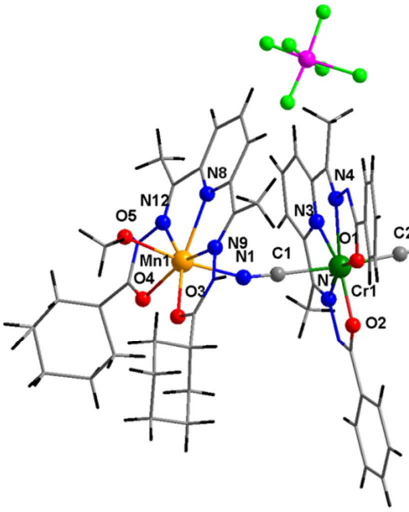

Figure 1. Molecular structure of the dinuclear complex $[Cr(L)(CN)_2Mn(H_2L^1)(MeOH)](PF_6)\cdot H_2O\cdot 2MeOH$, **1** omitting the crystallographic disorder on a cyclohexyl group and the solvent molecules.

The crystal structure for the chain $[Cr(L)(CN)_2Mn(H_2L^2)](PF_6)$ (**2**) confirmed the formation of a coordination polymer (Figure 2) constituted of alternating Cr and Mn centers linked by the cyanide ligands associated to an PF_6^- anion and crystallized with solvent molecules (2 H_2O and 1 MeOH molecules). The Cr and Mn centers are heptacoordinated with a pentagonal bipyramid polyhedral shape (Figure 2 and Table S1). The axial positions of the manganese ion are occupied by the nitrogen atoms of the bridging cyanides (Mn1–N = 2.197 to 2.230 Å). The chains are slightly bent with average Mn–N–C angle close to 158.5° and Cr–C–N angles of 175°. The chains propagate along the *a* axis (Figures S3b and S3c); the shortest inter-chain metal-metal separation is found between two Mn atoms separated by 8.81 Å.

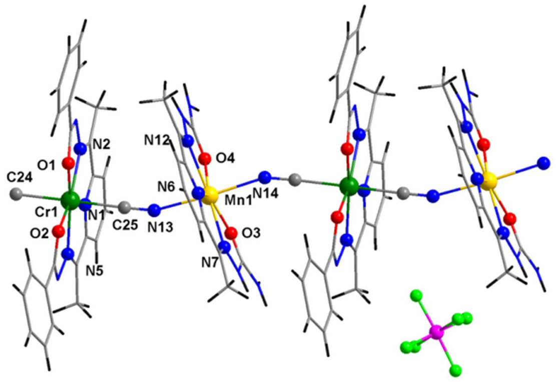

Figure 2. Molecular structure of the chain $[Cr(L)(CN)_2Mn(H_2L2)](PF_6)\cdot 2H_2O\cdot MeOH$, **2**. The solvates and one counter-ion are not shown for clarity.

The compounds **3** and **4** are also cyanide-bridged Cr-Mn cationic chains (Figures 3 and S5). Their charge is this time compensated by a chromium complex and they crystallized with solvent molecules (5.5 H_2O and 3 MeOH for **3** and 6 water molecules for **4**). The chains display a similar molecular arrangement with closely related bond distances and angles (Tables S6, S7, S8 and S9). They are quite linear with average Mn–N–C and Cr1–C–N angles of 160.5/172.7° (**3**); 161/172.4° (**4**). The steric hindrance of the peripheral group on the Mn site is the main difference resulting in an almost perpendicular orientation of the mandelic groups with both substituents on the same side *vs*. the pentadentate plane (Figure 3) while the core of the H_2L^3 ligand is perfectly planar in **3** (Figure S5). The chains are propagating along the *a* axis and are packed in layers in the (*a*,*b*) plane with the anions intercalated between the layers (Figures S7b and Figure S7c). The shortest metal-metal distance is 8.75 Å for **3** between Cr atoms of adjacent chains (Figure S5c) while it equals 9.00 Å for **4** between Cr atoms of the anion and Mn sites of the chain (Figure S7c). Finally, these two chains crystallized in chiral space groups which is not surprising for **4** as we started from a chiral building block. In **3**, we can exclude any spontaneous resolution effect as we did not observe the presence of CD signals from solid state circular dichroism measurement (Figure S8). This compound crystallized then as a racemic mixture.

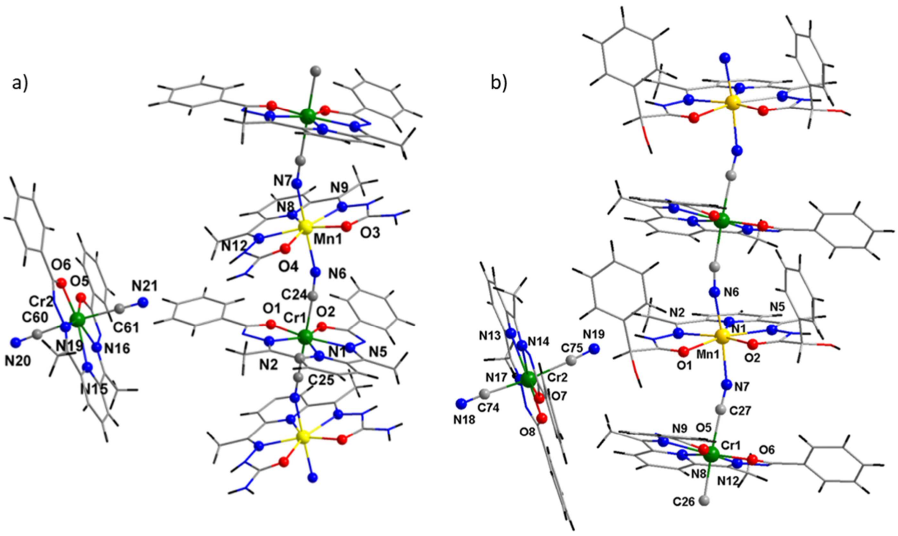

Figure 3. Molecular structure of the chains a) $[Cr(L)(CN)_2Mn(H_2L2)][Cr(L)(CN)_2]$, **3** and b) $[Cr(L)(CN)_2Mn(H_2L3)][Cr(L)(CN)_2]$, **4**. The solvates are not shown for clarity.

The phase purity of the compounds was checked by Powder X-Ray Diffraction (PXRD) as shown on Figures S2, S4, S6 and S9. Experimental and calculated diffractograms are globally well superposed except small diffraction peaks corresponding to trinuclears for **3** and **4**. It was not possible to get samples without these additional traces of trinuclear complexes, most certainly because the stoechiometry 2 :1 between Cr and Mn is common for the discrete and 1D species.

Magnetic properties. The dc magnetic susceptibility (χ_M stands for the molar magnetic susceptibility) versus temperature and the magnetization (*M*) versus field were investigated for all compounds to probe the impact of substituents on intra- and inter-molecular exchange interactions.

For the dinuclear system **1**, the $\chi_M T$ product was 5.98 cm^{3}Kmol^{-1} at 300 K. A theoretical Curie contribution of 6.25 cm^{3}Kmol^{-1} is expected for one Cr(III) and one Mn(II) in the absence of exchange interactions. This value decreased to 1.65 cm^{3}Kmol^{-1} at 3.6 K followed by a slight increase to 1.77 cm^{3}Kmol^{-1} at 2 K (Figure 4). Such a behavior is characteristic for an antiferromagnetic Cr-Mn interaction, in agreement with similar cyanido-bridged Cr-Mn systems.[5] The resulting $S = 1$ ground spin state implies a $\chi_M T$ signal tending to 1 cm^{3}Kmol^{-1}, which is not reached for **1**. The larger experimental values combined with the slight increase below 5 K are reproducible as two batches showed these features. Contamination of the samples by traces of a chain derivative is discarded by PXRD (see Figure S2). The observed behavior can be attributed to intermolecular interactions by means of the hydrogen bonds linking Cr and Mn sites of adjacent molecules (Figure S1b). Modeling of the thermal dependence of $\chi_M T$ was performed with an expression of the susceptibility derived from the Hamiltonian given equation 2. The contribution of intermolecular interactions was considered in the mean-field approximation.[12] The best fit to the experimental behavior yielded $J = -6.36 \pm 0.06$ cm^{-1}, $g = 1.97 \pm 0.01$, $zJ' = +0.27 \pm 0.02$ cm^{-1}. The strength of the Cr-Mn exchange interaction is similar to reported values.[5] The magnetization (*M*) curve at 2 K of **2** (Figure S11) shows a very fast increase of the magnetization for weak fields and a smoother variation for higher field tending to 2.13 μ_B, close to 2 μ_B expected for a $S = 1$ ground state.

$\widehat{H} = -J(\hat{S}_{Mn}.\hat{S}_{Cr})$ (Equation 1) with *J* the exchange interaction between Mn and Cr sites

$\chi = \chi_{CrMn} / \left[1 - \left(\frac{zj'}{Ng^2\mu_B^2}\right)\chi_{CrMn}\right]$ (Equation 2) where *zj'* is the intermolecular interaction, *N* is the Avogadro number, *g* is the Landé factor and μ_B is the Bohr magneton.

For the 1D compounds **2**, **3** and **4**, the magnetic features are characteristic of ferrimagnetic spin chains (Figures 4 and S9). The $\chi_M T$ values found at 300 K are respectively, 5.79, 4.45 and 7.72 cm^{3}mol^{-1}K. Upon cooling, this value decreases to a minimum around respectively, 13, 10 and 16 K before increasing steeply for lower temperatures (Figure S10). The classical model developed for an Heisenberg linear chain with alternating spins[13] was used to reproduce these magnetic behaviors. A good agreement with the experimental data was reached with the following sets of parameters: $J = -5.97 \pm 0.05$ cm^{-1} and $g = 1.98 \pm 0.01$ for **2**, $J = -5.06 \pm 0.05$ cm^{-1} and $g = 1.97 \pm 0.01$ for **3** and $J = -7.46 \pm 0.09$ cm^{-1} and $g = 1.98 \pm 0.01$ for **4** (Figures 4 and S11). These values of Cr(III)-Mn(II) exchange interactions are similar with the ones found in homologous heptacoordinated[6,7b] systems and are in the same range of order compared to cyanide-bridged hexacoordinated Cr-Mn species.[14] The magnetization for **2** is characterized by an S-shaped trace with a slop bending at 830 Oe before a rapid increase of *M* to reach saturation value of 2.16 μ_B (Figure S11a), suggesting a metamagnetic behavior. To probe this effect, χ_M as a function of the temperature was measured under different fields between 100 and 4000 Oe (Figure S12a) and magnetization curves were recorded between 3 and 8 K (Figure S12b). The phase diagram (*H*,*T*) was constructed from the maxima on χ *vs.* *T* and d*M*/d*H* *vs.* *H* curves (Figure 5). This metamagnetic behavior is likely the result of weak interchain interaction attributed to the short separation between the chains. Here the peripheral groups of the ligand play an important role, for **2** the steric hindrance of the NH_2 groups is not sufficient to screen the intermolecular exchange interactions between the chains.

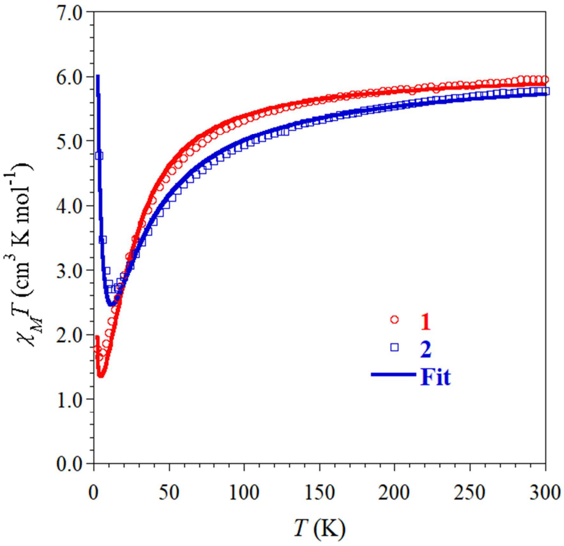

Figure 4. Experimental (O/☐) and calculated (—) temperature dependence of $\chi_M T$ for **1** and **2**, the best fit parameters are discussed in the text.

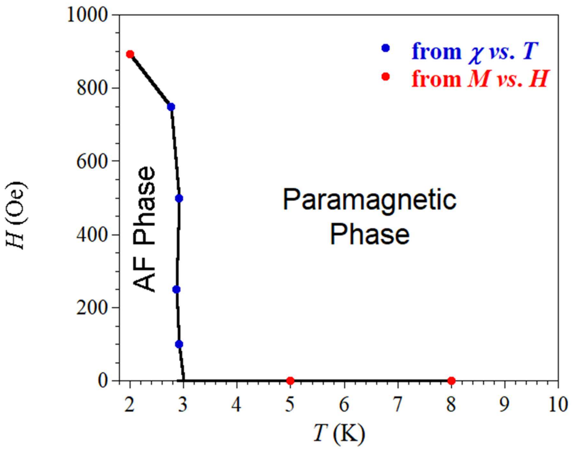

Figure 5. Phase diagram (*H*,*T*) for *2*. The black line is a guide for the eyes.

The magnetization value for **3** and **4** at 5 Tesla is respectively 4.85 and 5 μ_B corresponding to a ground state $S = 1$ of the CrMn chain subunit plus the contribution of the Cr anion ($S = 3/2$). For these chains, no metamagnetic behavior was observed (Figure S11b).

These magnetic systems validate the strength of Cr-CN-Mn exchange interactions previously determined in trinuclear complexes[7b] but also underline the importance of bulky substituents to shortcut interchain exchange pathways with diamagnetic scaffolds screening the exchange interactions.

CONCLUSION

The pentadentate ligands considered herein are interesting platforms to synthesize heptacoordinated complexes with various functional groups (R) at the periphery. These substituents allow introducing in the complexes an additional functionality like chirality[7b,15] but they also appear to play an important role during the crystallization process. This work and our previous results[7] illustrate the subtle effect of R on the selective crystallization of discrete or 1D heterometallic compounds possibly formed during the assemblage progression. Reagents stoichiometry and solvent conditions are the experimental parameters chemists typically adjust to target a product but the species actually crystallizing is also driven by solubility considerations; and this can be greatly dependent on the R substituents as illustrated in this study.

The R groups also contribute to the crystal packings and hence the intra- and inter-molecular contacts. The first may mostly contribute to the bending of the polynuclear compounds[7b] while the seconds are promoting additional pathways for magnetic interactions, but both contribute to the overall magnetic behaviors of the compounds.

Within this family of ligands, the R-substituents should be considered as an additional parameter with which chemists can fine-tune the selectivity of the reaction and the magnetic behavior.

EXPERIMENTAL SECTION.

Materials and methods: All reagents and solvents were used as received from commercial sources. The complexes $[Mn(H_2L^1)Cl_2].0.5H_2O$, $[Mn(H_2L^2)Cl_2].2H_2O$ and $[Mn(H_2L^3)Cl_2]\cdot 2H_2O$ were prepared following the reported procedures.[7b] Fourier transform infrared (FT-IR) spectroscopy was performed with a Perkin–Elmer spectrum GX 2000 FT-IR spectrometer. Elemental analyses were performed with a Perkin–Elmer 2400 series II instrument. Magnetic susceptibility measurements were carried out with a Quantum Design MPMS-5S SQUID magnetometer. The magnetic studies were performed on freshly isolated polycrystalline powders put in gelatin capsules. Data have been collected between 300 and 2 K with an applied field of 1 kOe and corrected for the diamagnetic contribution sample by using Pascal's tables[16] and for the sample holder. The field dependences of the magnetization were measured at 2 K with dc magnetic field up to 5 T. The absence of ferromagnetic impurities was checked by measurement of M *vs.* H at 100 K. The Circular Dichroism (CD) spectrum was recorded with a Jacso J-815 spectropolarimeter on pellets of compound diluted in KBr (1.25 % of compound). The experiment was performed at room temperature in a 900-300 nm wavelength range, 2 nm data pitch, 1 nm bandwidth, 100 nm/min scanning speed, continuous scanning mode, 4 s DIT and no accumulation.

Syntheses:

$[Cr(L)(CN)_2Mn(H_2L^1)(MeOH)](PF_6)\cdot H_2O\cdot 2MeOH$, **1**: A solution of $K[Cr(L)(CN)_2]\cdot 2H_2O$ (0.015 g, 0.03 mmol) in 0.5 mL MeOH was placed in a 1 cm diameter tube. $[Mn(H_2L^1)Cl_2].0.5H_2O$ (0.013 g, 0.02 mmol) dissolved in MeOH (0.5 mL) was slowly layered on the top. Orange crystals were isolated after 1 night. Yield: 11 mg (30 %). IR (KBr, cm^{-1}): 3351 (w), 3210 (w), 2932 (m), 2857 (m), 2150 (w), 2127 (sh), 1651 (m), 1637 (m), 1586 (m), 1561 (m), 1519 (s), 1494 (sh), 1451 (m), 1433 (m), 1382 (s), 1341 (w), 1304 (w), 1266 (m), 1199 (sh), 1177 (m), 1136 (sh), 1104 (w), 1084 (w), 1071 (w), 1048 (m), 1025 (w), 1014 (w), 994 (w), 953 (w), 846 (s), 810 (sh), 740 (w), 714 (m), 683 (m). Elemental analysis (%) calcd. for $C_{50}H_{62}CrF_6MnN_{12}O_7P$ ($[Cr(L)(CN)_2Mn(H_2L^1)(MeOH)](PF_6)\cdot H_2O$): C 50.25; H 5.23; N 14.07; found: C 50.11; H 5.09; N 13.75.

$[Cr(L)(CN)_2Mn(H_2L^2)](PF_6)\cdot 2H_2O\cdot MeOH$, **2**: $K[Cr(L)(CN)_2]$ (0.044 g, 0.07 mmol) in 10 mL MeOH was added dropwise to $[Mn(H_2L^2)Cl_2].2H_2O$ (0.064 g, 0.15 mmol) and NH_4PF_6 (0.8 g, 0.49 mmol) dissolved in 6 mL H_2O and 6 mL MeOH. A red/brown solid slowly appeared during the addition. The suspension was stirred overnight at room temperature. The polycrystalline solid was filtered and washed with MeOH (4 mL) followed by Et_2O (5 mL), yielding 58 mg (79 % based on Cr) of **2**. Phase purity of this polycrystalline solid was confirmed by PXRD, see Figure S4. Conditions to get single crystals suitable for X-ray structure analysis: A solution of $[Mn(H_2L^2)Cl_2]$ (0.014 g, 0.03 mmol) and NH_4PF_6 (0.02 g, 0.12 mmol) in 1 mL H_2O and 1 mL MeOH was placed in a 1 cm diameter hemolysis tube and layered with 2 mL of H_2O/MeOH (1:1). A solution of $[Cr(L)(CN)_2]K$ (0.007 g, 0.012 mmol) in 2 mL MeOH was carefully added on the top. After 2 days, dark orange crystals appeared. IR (KBr, cm^{-1}): 3643 (w), 3521 (m), 3401 (m), 3350 (m), 3274 (sh), 3205 (sh), 2919 (m), 2153 (w), 2148 (w), 1682 (m), 1634 (w), 1614 (w), 1601 (w), 1586 (w), 1558 (sh), 1519 (s), 1495 (sh), 1455 (w), 1435 (w), 1419 (w), 1379 (s), 1306 (w), 1270 (w), 1214 (sh), 1196 (m), 1179 (w), 1163 (w), 1149 (w), 1138 (w), 1122 (w), 1096 (m), 1073 (w), 1051 (m), 1025 (w), 1013 (w), 938 (sh), 907 (w), 844 (s), 817 (sh), 812 (w), 802 (w), 758 (w), 739 (w), 716 (m), 685 (w), 645 (w). Elemental analysis (%) calcd. for $C_{36}H_{36}CrF_6MnN_{14}O_5P$ ($[Cr(L)(CN)_2Mn(H_2L^2)](PF_6)\cdot H_2O$): C 43.38; H 3.64; N 19.68; found: C 43.59; H 3.60; N 19.55.

$[Cr(L)(CN)_2Mn(H_2L^2)][Cr(L)(CN)_2]\cdot 5.5H_2O\cdot 3MeOH$, **3**: A solution of $[Mn(H_2L^2)Cl_2].2H_2O$ (0.036 g, 0.10 mmol) in 4 mL H_2O was placed in a 1 cm diameter tube and layered with 2 mL of H_2O/MeOH 50:50. $K[Cr(L)(CN)_2]$ (0.040 g, 0.06 mmol) dissolved in 4 mL MeOH was layered on top. Orange crystals were isolated after 3 days which were filtered and washed with MeOH (4 mL) followed by Et_2O (5 mL), yielding 12 mg (10 % based on Cr) of **3**. IR (KBr, cm^{-1}): 2963 (w), 2927 (w), 2908 (w), 2160 (w), 2151 (sh), 1674 (m), 1634 (m), 1599 (w), 1587 (w), 1516 (m), 1494 (w), 1454 (w), 1417 (w), 1373 (m), 1259 (s), 1196 (w), 1162 (w), 1091 (m), 1015 (m), 838 (sh), 785 (s), 738 (m), 712 (m), 683 (m).

Elemental analysis (%) calcd. for $C_{61}H_{61}Cr_2MnN_{21}O_{10}$ ($[Cr(L)(CN)_2Mn(H_2L^2)][Cr(L)(CN)_2]\cdot 4H_2O$): C 52.06; H 4.37; N 20.90; found: C 52.12; H 3.78; N 20.13.

***$[Cr(L)(CN)_2Mn(H_2L^3)][Cr(L)(CN)_2]\cdot 6H_2O$*, 4**: $[Mn(H_2L^3)Cl_2]\cdot 2H_2O$ (0.022 g, 0.03 mmol) in 6 mL MeOH was added dropwise to a solution of $K[Cr(L)(CN)_2]\cdot 2H_2O$ (0.045 g, 0.08 mmol) in 9 mL H_2O. An orange solid slowly appeared during the addition. The suspension was stirred overnight at room temperature. The solid was filtered and washed with a minimum of a mixture H_2O/MeOH 50:50 followed by Et_2O (5 mL), yielding 58 mg (91 % based on Cr) of **4**. Based on PXRD, this orange polycrystalline solid incorporated a small amount of the trinuclear complex $\{Cr_2Mn(L^3)\}$[7b], see Figure S6. Conditions to grow single crystals suitable for X-ray data collection: a solution of $K[Cr(L)(CN)_2]\cdot 2H_2O$ (0.015 g, 0.03 mmol) in 3 mL H_2O was placed in a 1 cm diameter tube and layered with 1 mL of H_2O/MeOH 50:50. $[Mn(H_2L^3)Cl_2]\cdot 2H_2O$ (0.007 g, 0.01 mmol) dissolved in MeOH (2 mL) was slowly layered on the top. Orange single crystals suitable for X-ray data collection were isolated after 2 days. Yield: 6 mg (28 %). IR (KBr, cm^{-1}): 2161 (w), 2133 (w), 2128 (sh), 1673 (m), 1645 (m), 1586 (m), 1558 (m), 1519 (s), 1494 (m), 1421 (m), 1381 (s), 1351 (sh), 1304 (w), 1278 (w), 1304 (w), 1235 (w), 1202 (w), 1175 (m), 1160 (sh), 1047 (w), 994 (w), 905 (w), 806 (w), 737 (w), 737 (w), 714 (w), 683 (w). Elemental analysis (%) calcd. for $C_{75}H_{75}Cr_2MnN_{19}O_{14}$ ($[Cr(L)(CN)_2Mn(H_2L^3)][Cr(L)(CN)_2]\cdot 6H_2O$): C 55.42; H 4.65; N 16.37; found: C 55.15; H 4.39; N 16.07.

Single-crystal X-ray diffraction: Single crystals suitable for X-ray diffraction were coated with paratone oil and mounted onto the goniometer. The X-ray crystallographic data were obtained at low temperature from an Apex2 Bruker (MoKα radiation source) or a Gemini Oxford-Diffraction (CuKα radiation source) diffractometer, equipped with an Oxford Cryosystem. The structures have been solved by direct methods using Superflip and refined by means of least-square procedures on F using the PC version of the program CRYSTALS. The scattering factors for all the atoms were used as listed in the International Tables for X-ray Crystallography. Absorption correction was performed using a multi-scan procedure. When it was possible, all non-hydrogen atoms were refined anisotropically. The H atoms were usually located in a difference map except some on solvate molecules, but those attached to carbon atoms were systematically repositioned geometrically. The H atoms were initially refined with soft restraints on the bond lengths and angles to regularize their geometry and Uiso (H) (in the range 1.2-1.5 times Ueq of the parent atom), after which the positions were refined with riding constraints. For **3**, it was not possible to resolve some diffuse electron-density residuals (enclosed solvent molecules). Some solvent molecules were squeezed with the SQUEEZE facility from PLATON: $2.5H_2O \cdot 1MeOH$ (per asymmetric unit). The structure for **1** presented a statistic disorder that concerns part of one ligand and a PF_6^- anion. The crystal of **4** was poorly diffracting, leading to a lack of data at high angle and a low theta full. However Crystallographic informations for all the complexes are gathered in Table 1; the CIF files are also available from The Cambridge Crystallographic Data Centre (www.ccdc.cam.ac.uk/data_request/cif) under the references CCDC-2095429 to 2095432. ORTEP plots and selected bond distances and angles are given in the supporting information.

Powder X-Ray diffraction (PXRD) patterns were recorded in transmission mode using capillary tubes on a XPert Pro (Theta–Theta mode) Panalytical diffractometer with $\lambda(Cu_{K\alpha1,K\alpha2})$ = 1.54059 and 1.54439 Å.

SUPPORTING MATERIAL

Crystallographic and geometric information; polyhedral shape analyses of the coordination spheres; powder X-ray diffraction diagrams and additional magnetic data. The crystallographic information for the structures has been deposited at CCDC with references CCDC-2095431 (**1**), CCDC-2095430 (**2**), CCDC-2095429 (**3**), CCDC-2095432 (**4**). These data can be obtained free of charge from The Cambridge Crystallographic Data Centre via www.ccdc.cam.ac.uk/data_request/cif.

ACKNOWLEDGEMENTS

This work was supported by the French National Research Agency, ANR, (grant ANR-17-CE07-0007). Authors are grateful to J.-F. Meunier, Laure Vendier (LCC) and Charles-Louis Serpentini (IMRCP) for technical assistance in magnetic, powder X-Ray data and CD collections, respectively.

Table 1. Selected crystallographic data and refinement parameters of **1**-**5**.

	1	**2**	**3**	**4**
Formula[a]	$C_{51}H_{65}CrF_6MnN_{12}O_8P$	$C_{37}H_{42}CrF_6MnN_{14}O_7P$	$C_{63}H_{67}Cr_2MnN_{21}O_{11}$	$C_{75}H_{75}Cr_2MnN_{19}O_{14}$
Mw (g.mol^{-1})	1226.04	1046.72	1453.28	1625.46
Crystal system	Monoclinic	Monoclinic	Monoclinic	Triclinic
Space group	$P2_1/c$	$P2_1/c$	Pc	P1
T (K)	180	100	100	123
a (Å)	14.772(3)	10.688(1)	21.005(1)	10.287(1)
b (Å)	17.671(2)	25.152(1)	10.750(1)	10.548(1)
c (Å)	23.482(4)	16.853(1)	16.763(1)	19.439(1)
α (°)	90	90	90	75.152(1)
β (°)	91.024(5)	103.299(2)	96.030(2)	76.839(1)
γ (°)	90	90	90	83.95(1)
V (Å^3)	6128.6(20)	4409.3(3)	3764.3(3)	1982.8(1)
Z	4	4	2	1
$\rho_{calcd.}$ (g cm^{-3})	1.33	1.58	1.28	1.36
μ (mm^{-1})	0.486 (Mo Kα)	0.660 (Mo Kα)	0.516 (Mo Kα)	4.112 (Cu Kα)
Collected reflns	63446	94579	133493	32202
Unique reflns	13382	9047	20914	10169
R_{int}	0.107	0.064	0.047	0.026
Nb of parameters	703	604	884	1010
Nb of reflns($I \geq n\sigma$)	7049, n=2.1	6801, n=3	18046, n=3	9750, n=3
Final R_1, wR_2 ($I \geq n\sigma$)[b,c]	0.0885, 0.0714	0.0361, 0.0367	0.0340, 0.0363	0.0394, 0.0474
Flack parameter	/	/	0.002(7)	0.001(3)
$\Delta\rho_{min}$/ $\Delta\rho_{max}$	-0.79/1.40	-0.53/0.73	-0.44/0.57	-0.24/1.42
GOF	0.83	1.062	1.082	0.954
CCDC number	2095431	2095430	2095429	2095432

[a] Including co-crystallized solvent molecules (except for **3** for which some solvent molecules were squeezed), [b] $R_1 = \Sigma||F_o| - |F_c||/\Sigma|F_o|$; [c] $wR_2 = [\Sigma(w(F_o^2 - F_c^2)^2)/\Sigma([w(F_o^2)^2]^{1/2}$ where $w = 1/(\sigma^2(F_o^2) + (aP)^2 + bP)$ with $P = (2F_c^2 + \max(F_o^2,0))/3$.

REFERENCES

---

[1] a) Y. Pei, O. Kahn, J. Sletten, *J. Am. Chem. Soc.* **1986**, *108*, 3143-3145; b) Y. Pei, M. Verdaguer, O. Kahn, J. Sletten, J. P. Renard, *J. Am. Chem. Soc.* **1986**, *108*, 7428-7430; c) H. O. Stumpf, L. Ouahab, Y. Pei, D. Grandjean, O. Kahn, *Science* **1993**, *261*; d) O. Kahn, *Acc. Chem. Res.* **2000**, *33*, 647-657; e) C. Milios, R. P. Winpenny, in *Molecular Nanomagnets and Related Phenomena, Vol. 164* (Ed.: S. Gao), Springer Berlin Heidelberg, **2015**, pp. 1-109; f) S. Dhers, H. L. C. Feltham, S. Brooker, *Coord. Chem. Rev.* **2015**, *296*, 24-44; g) M.-C. Dul, E. Pardo, R. Lescouëzec, Y. Journaux, J. Ferrando-Soria, R. Ruiz-García, J. Cano, M. Julve, F. Lloret, D. Cangussu, C. L. M. Pereira, H. O. Stumpf, J. Pasán, C. Ruiz-Péréz, *Coord. Chem. Rev.* **2010**, *254*, 2281-2296; h) J. Ferrando-Soria, J. Vallejo, M. Castellano, J. Martínez-Lillo, E. Pardo, J. Cano, I. Castro, F. Lloret, R. Ruiz-García, M. Julve, *Coord. Chem. Rev.* **2017**, *339*, 17-103; i) O. Kahn, *VCH: Weinheim* **1993**.

[2] a) M. Verdaguer, A. Bleuzen, V. Marvaud, J. Vaissermann, M. Seuleiman, C. Desplanches, A. Scuiller, C. Train, R. Garde, G. Gelly, C. Lomenech, I. Rosenman, P. Veillet, C. Cartier, F. Villain, *Coord. Chem. Rev.* **1999**, *190-192*, 1023-1047; b) K. S. Pedersen, J. Bendix, R. Clerac, *Chem. Commun.* **2014**, *50*, 4396-4415.

[3] a) T. S. Venkatakrishnan, S. Sahoo, N. Bréfuel, C. Duhayon, C. Paulsen, A.-L. Barra, S. Ramasesha, J.-P. Sutter, *J. Am. Chem. Soc.* **2010**, *132*, 6047-6056; b) N. Gogoi, M. Thlijeni, C. Duhayon, J.-P. Sutter, *Inorg. Chem.* **2013**, *52*, 2283-2285; c) R. Ruamps, L. J. Batchelor, R. Maurice, N. Gogoi, P. Jiménez-Lozano, N. Guihéry, C. de Graaf, A.-L. Barra, J.-P. Sutter , T. Mallah, *Chem. Eur. J.* **2013**, *19*, 950-956; d) X.-C. Huang, C. Zhou, D. Shao, X.-Y. Wang, *Inorg. Chem.* **2014**, *53*, 12671-12673; e) A. K. Bar, C. Pichon, N. Gogoi, C. Duhayon, S. Ramasesha, J.-P. Sutter, *Chem. Commun.* **2015**, *51*, 3616-3619; f) P. Antal, B. Drahoš, R. Herchel, Z. Trávníček, *Inorg. Chem.* **2016**, *55*, 5957-5972; g) M. Dey, S. Dutta, B. Sarma, R. C. Deka, N. Gogoi, *Chem. Commun.* **2016**, *52*, 753-756; h) D. Shao, S.-L. Zhang, L. Shi, Y.-Q. Zhang, X.-Y. Wang, *Inorg. Chem.* **2016**, *55*, 10859-10869; i) A. K. Bar, N. Gogoi, C. Pichon, V. M. L. D. P. Goli, M. Thlijeni, C. Duhayon, N. Suaud, N. Guihéry, A.-L. Barra, S. Ramasesha, J.-P. Sutter, *Chem. Eur. J.* **2017**, *23*, 4380-4396.

[4] a) Y.-S. Ding, N. F. Chilton, R. E. P. Winpenny, Y.-Z. Zheng, *Angew. Chem. Int. Ed.* **2016**, *55*, 16071–16074; b) J. Liu , Y.-C. Chen, J.-L. Liu, V. Vieru, L. Ungur, J.-H. Jia, L. F. Chibotaru, Y. Lan, W. Wernsdorfer, S. Gao, X.-M. Chen, M.-L. Tong, *J. Am. Chem. Soc.* **2016**, *38*, 5441–5450; c) Z. Jiang, L. Sun, Q. Yang, B. Yin, H. Ke, J. Han, Q. Wei, G. Xie, S. Chen, *J. Mater. Chem. C* **2018**, *6*, 4273–4280; d) A. B. Canaj, S. Dey, C. Wilson, O. Céspedes, G. Rajaraman, M. Murrie, *Chem. Commun.* **2020**, *56*, 12037–12040.

[5] E. L. Gavey, M. Pilkington, *Coord. Chem. Rev.* **2015**, *296*, 125-152.

[6] C. Pichon, B. Elrez, V. Béreau, C. Duhayon, J.-P. Sutter, *Eur. J. Inorg. Chem.* **2018**, *2018*, 340-348.

[7] a) C. Pichon, N. Suaud, C. Duhayon, N. Guihéry, J.-P. Sutter, *J. Am. Chem. Soc.* **2018**, *140*, 7698-7704; b) C. Pichon, N. Suaud, V. Jubault, C. Duhayon, N. Guihéry, J.-P. Sutter, *Chem. Eur. J.*, **2021**, *27*, 15484.

[8] K. Bretosh, V. Béreau, C. Duhayon, C. Pichon, J.-P. Sutter, *Inorg. Chem. Front.* **2020**, *7*, 1503-1511.

[9] O. Jimenez-Sandoval, D. Ramirez-Rosales, M. del Jesus Rosales-Hoz, M. Elena Sosa-Torres, R. Zamorano-Ulloa, *J. Chem. Soc., Dalton Trans.* **1998**, 1551-1556.

[10] a) D. Casanova, P. Alemany, J. M. Bofill, S. Alvarez, *Chem. Eur. J.* **2003**, *9*, 1281; b) S. Alvarez, P. Alemany, D. Casanova, J. Cirera, M. Llunell, D. Avnir, *Coord. Chem. Rev.* **2005**, *249*, 1693-1708.

[11] M. C. Llunell, D.; Cirera, J.; Alemany, P.; Alvarez, S., *Shape program, version 2; Universitat de Barcelona: Barcelona, Spain* **2013**.

[12] C. J. O'Connor, *Prog. Inorg. Chem.* **1982**, *29*, 203-283.

[13] M. Drillon, E. Coronado, D. Beltran, R. Georges, *Chem. Phys.* **1983**, *79*, 449-453.

[[14]] a) Z.-H. Ni, H.-Z. Kou, L. Zheng, Y.-H. Zhao, L.-F. Zhang, R.-J. Wang, A.-L . Cui, O. Sato, *Inorg. Chem.* **2005**, *44*, 4728–4736; b) G.-L. Li, L.-F. Zhang, Z.-H. Ni, H.-Z. Khou, A.-L. Cui, *Bull. Korean Chem. Soc.* **2012**, *33*, 1675–1680; c) Z.-H. Ni, L.-F. Zhang, C.-H. Ge, A.-L. Cui, H.-Z. Kou, J. Jiang, *Inorg. Chem. Commun.* **2008**, *11*, 94–96.

[15] A. Choudhury, C. Pichon, J.-P. Sutter, D. Pamu, B. Sarma, P. P. Mudoi, N. Gogoi, *Chem. Commun.* **2021**, *57*, 207-210.

[16] O. Kahn, *Molecular Magnetism*, VCH, Weinheim, **1993**.

Discrete *versus* 1D compounds based on pentagonal bipyramid coordination geometries: a matter of solubility?

TABLE OF CONTENT.

Table S1. Results of Continuous Shape Measures calculation using SHAPE[1] with the closest geometries for each metal center highlighted in blue.

Heptacoordinated centers[2]

HP-7	D_{7h}	Heptagon
HPY-7	C_{6v}	Hexagonal pyramid
PBPY-7	D_{5h}	Pentagonal bipyramid
COC-7	C_{3v}	Capped octahedron
CTPR-7	C_{2v}	Capped trigonal prism
JPBPY-7	D_{5h}	Johnson pentagonal bipyramid J13
JETPY-7	C_{3v}	Johnson elongated triangular pyramid J7

Metal center	HP-7	HPY-7	PBPY-7	COC-7	CTPR-7	JPBPY-7	JETBPY-7
Cr1@**1**	34.224	24.372	0.247	7.814	6.191	3.451	23.874
Mn1@**1**	32.231	22.221	0.718	7.096	5.355	3.515	21.209
Cr1@**2**	33.345	22.815	0.439	6.724	5.138	3.634	22.838
Mn1@**2**	32.962	22.724	0.468	7.451	5.597	3.625	22.067
Cr1@**3**	33.597	22.584	0.476	7.236	5.741	3.674	22.245
Cr2@**3**	34.275	24.121	0.281	7.862	6.117	3.467	23.735
Mn1@**3**	32.375	21.723	0.675	7.352	5.469	3.899	20.878
Cr1@**4**	32.399	23.590	0.522	6.568	4.662	3.645	22.559
Cr2@**4**	32.443	24.662	0.342	7.345	5.424	3.569	22.265
Mn1@**4**	32.910	19.315	1.177	6.822	5.229	3.748	19.904

---

[1] M. Llunell, D. Casanova, J. Cirera, P. Alemany, S. Alvarez, *SHAPE: Program for the stereochemical analysis of molecular fragments by means of continuous shape measures and associated tools*, 2.1; University of Barcelona: Barcelona, 2013.

[2] D. Casanova, P. Alemany, J. M. Bofill, S. Alvarez, *Chem. Eur. J.,* 2003, **9**, 1281

Figure S1. (a) Asymmetric unit of [Cr(L)(CN)$_2$Mn(H$_2$L^1)(MeOH)](PF$_6$), **1** with thermal ellipsoids fixed at 30 %. Crystal packing of **1** highlighting the organization by pairs with views (b) in the (*b*,*c*) plane and (c) in the (*a*,*c*) plane. The dashed red lines materialize the shortest intermolecular metal-metal distance (indicated in Å). Color scheme: C = grey, N = blue, O = red, Cr = green, Mn = yellow.

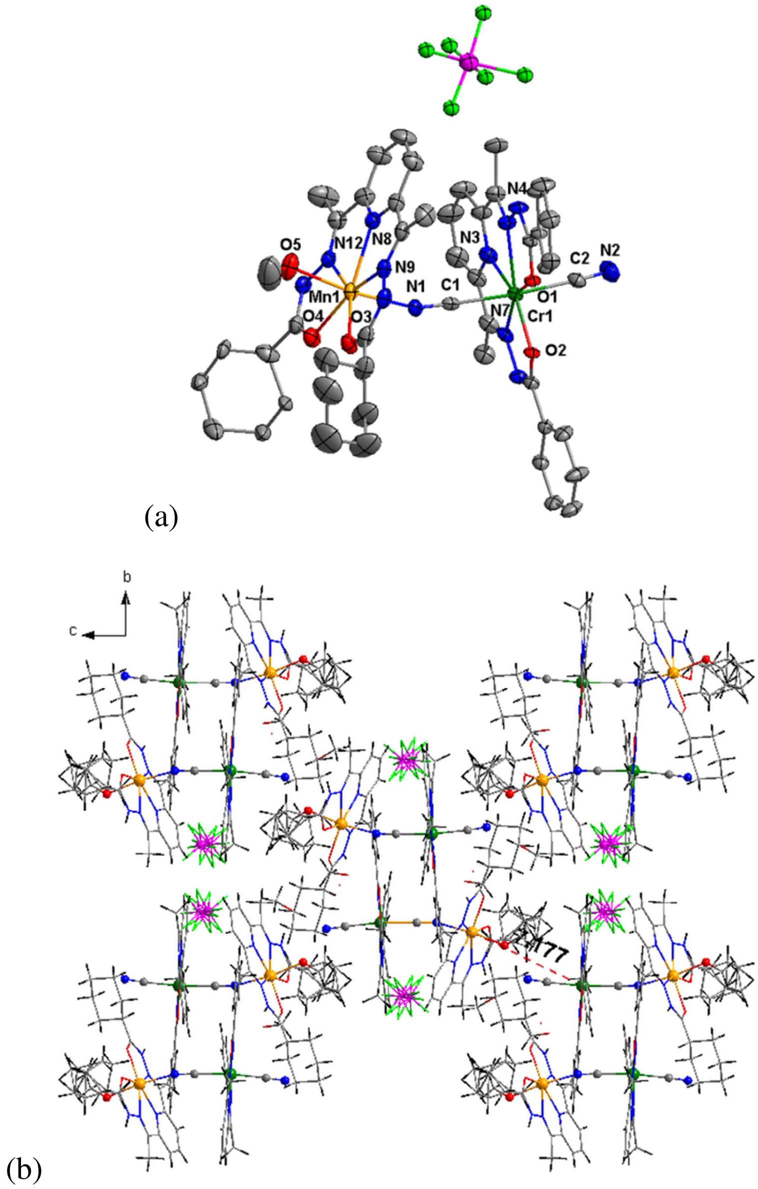

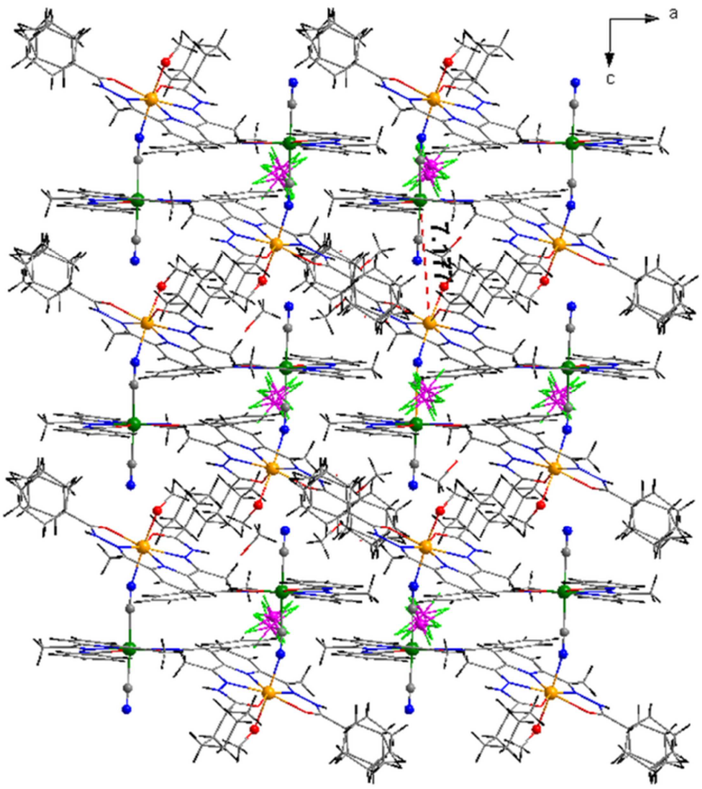

(c)

Table S2. Selected bond lengths of **1** (Å).

Cr1–C1	2.095(6)	Cr1–C2	2.085(6)	Cr1–N8	2.390(4)
Cr1–N4	2.235(4)	Cr1–N7	2.173(4)	Cr1–O1	1.980(3)
Cr1–O2	1.956(3)	Mn1–N1	2.210(5)	Mn1–N8	2.300(5)
Mn1–N9	2.307(4)	Mn1–N12	2.293(4)	Mn1–O3	2.245(4)
Mn1–O4	2.228(4)	Mn1–O5	2.200(5)		

Table S3. Selected bond angles of **1** (°).

C1–Cr1–C2	173.8(2)	C1–Cr1–N3	87.88(17)
C2–Cr1–N3	86.01(19)	C1–Cr1–N4	89.72(18)
C2–Cr1–N4	86.9(2)	N3–Cr1–N4	64.79(14)
C1–Cr1–N7	90.61(16)	C2–Cr1–N7	87.75(18)
N3–Cr1–N7	66.52(15)	N4–Cr1–N7	131.26(15)
C1–Cr1–O1	91.36(15)	C2–Cr1–O1	92.54(17)
N3–Cr1–O1	137.23(54)	N4–Cr1–O1	72.45(13)
N7–Cr1–O1	156.22(15)	C1–Cr1–O2	92.46(17)
C2–Cr1–O2	92.80(19)	N3–Cr1–O2	140.53(13)
N4–Cr1–O2	154.63(13)	N7–Cr1–O2	74.01(14)
O1–Cr1–O2	82.23(12)	N1–Mn1–N8	86.02(17)
N1–Mn1–N9	89.77(15)	N8–Mn1–N9	68.01(16)
N1–Mn1–N12	92.61(16)	N9–Mn1–N12	135.58(17)
N1–Mn1–O3	97.26(16)	N8–Mn1–O3	137.23(15)

N9–Mn1–O3	69.37(16)	N12–Mn1–O3	153.36(15)
N1–Mn1–O4	97.60(15)	N8–Mn1–O4	137.15(15)
N9–Mn1–O4	153.97(16)	N12–Mn1–O4	69.26(15)
O3–Mn1–O4	84.90(15)	N1–Mn1–O5	172.5(2)
N8–Mn1–O5	86.5(2)	N9–Mn1–O5	87.68(16)
N12–Mn1–O5	84.30(17)	O3–Mn1–O5	88.46(18)
O4–Mn1–O5	87.73(18)	Cr1–C1–N1	177.1(4)
Cr1–C2–N2	177.2(6)	Mn1–N1–C1	160.4(4)

Figure S2. Comparison of the experimental powder X-ray diffractogram measured on polycrystalline powder introduced with their mother solution in capillary tube with the calculated ones of **1**.

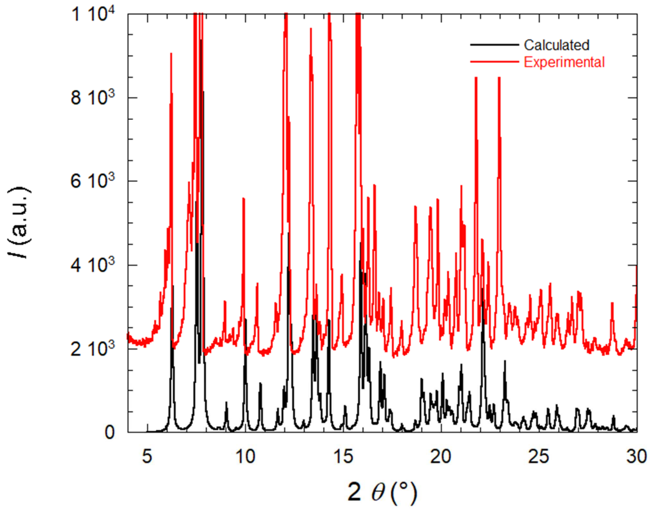

Figure S3. (a) Asymmetric unit of $[Cr(L)(CN)_2Mn(H_2L^2)](PF_6)\cdot 2H_2O\cdot MeOH$, **2** with thermal ellipsoids fixed at 30 % and without solvent molecules. Crystal packing of **2** (b) along the (*b*,*c*) plane perpendicularly to the chain propagation and (c) along the *a* axis. The dashed red lines materialize the shortest intermolecular metal-metal distance (indicated in Å). Color scheme: C = grey, H = black, N = blue, O = red, Cr = green, Mn = yellow.

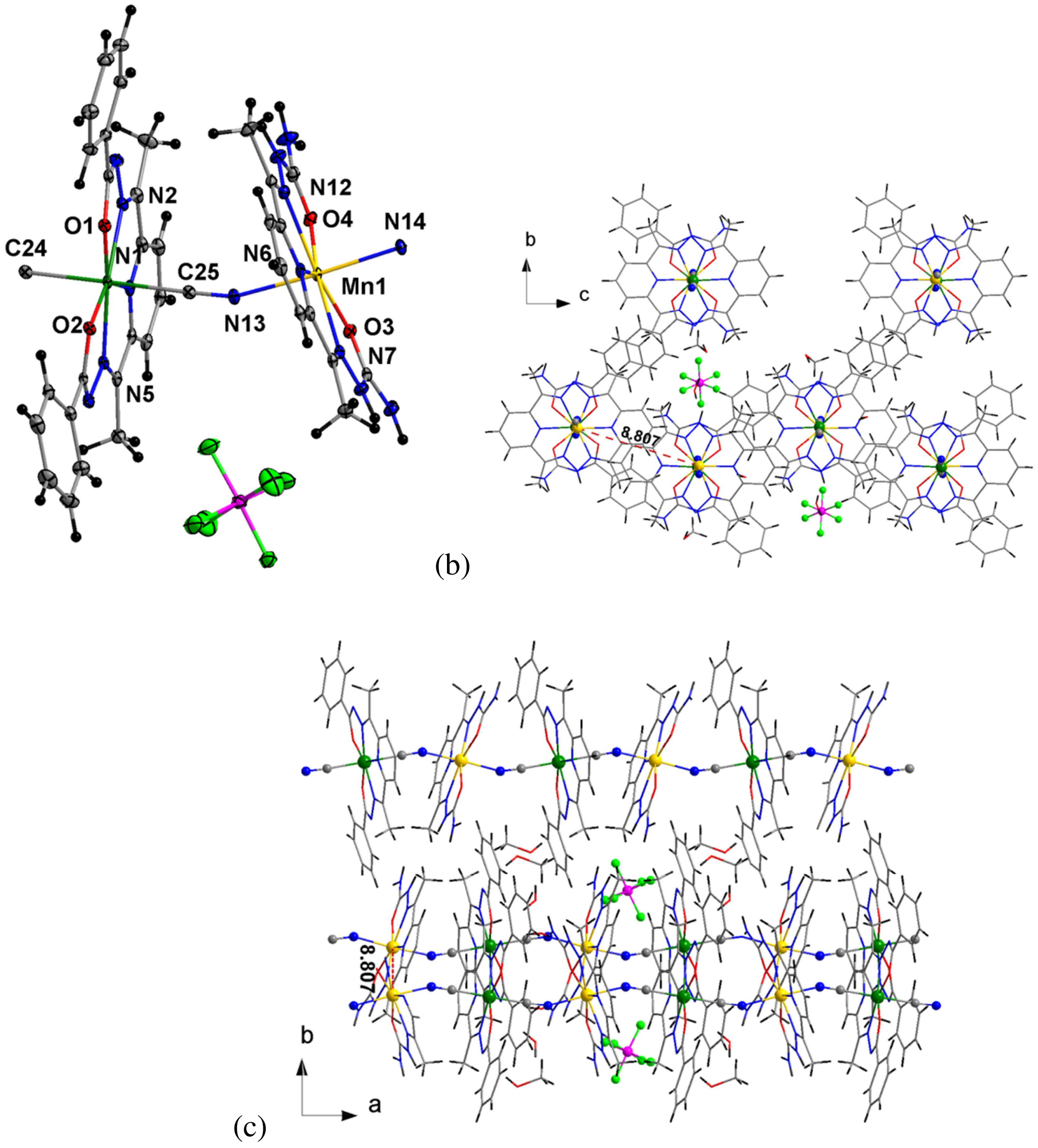

Table S4. Selected bond lengths of **2** (Å).

O1–Cr1	1.987(9)	O2–Cr1	1.958(1)	O3–Mn1	2.205(1)
O4–Mn1	2.258(5)	N1–Cr1	2.405(1)	N2–Cr1	2.224(2)
N5–Cr1	2.177(1)	N6–Mn1	2.320(2)	N7–Mn1	2.293(1)
N12–Mn1	2.313(2)	N13–Mn1	2.198(1)	N14–Mn1	2.230(1)
C24–Cr1	2.095(2)	C25–Cr1	2.085(2)		

Table S5. Selected bond angles of **2** (°).

C24–N14–Mn1	157.30(17)	N14–C24–Cr1	172.74(17)
O3–Mn1–N13	93.37(6)	O3–Mn1–N14	86.64(6)
N13–Mn1–N14	175.87(7)	O3–Mn1–O4	84.17(5)
N13–Mn1–O4	86.09(6)	N14–Mn1–O4	89.81(6)
O3–Mn1–N7	70.85(6)	N13–Mn1–N7	96.27(6)
N14–Mn1–N7	87.64(6)	O4–Mn1–N7	154.99(6)
O3–Mn1–N12	153.72(6)	N13–Mn1–N12	86.85(6)
N14–Mn1–N12	91.32(6)	O4–Mn1–N12	69.62(6)
N7–Mn1–N12	135.29(6)	O3–Cr1–N6	138.44(6)
N13–Mn1–N6	91.93(6)	N14–Mn1–N6	90.80(6)
O4–Mn1–N6	137.34(6)	N7–Mn1–N6	67.60(6)
N12–Mn1–N6	67.72(6)	N2–Cr1–N5	130.94(6)
N2–Cr1–C24	89.10(7)	N5–Cr1–C24	90.10(7)
N2–Cr1–C25	90.60(7)	N5–Cr1–C25	88.99(7)
C24–Cr1–C25	178.50(8)	N2–Cr1–N1	65.21(6)
N5–Cr1–N1	65.91(6)	C24–Cr1–N1	93.73(6)
C25–Cr1–N1	84.82(7)	N2–Cr1–O1	72.64(6)
N5–Cr1–O1	156.42(6)	C24–Cr1–O1	90.27(7)
C25–Cr1–O1	91.04(7)	N1–Cr1–O1	137.56(6)
N2–Cr1–O2	155.08(6)	N5–Cr1–O2	73.90(6)
N1–Cr1–O2	139.71(6)	O1–Cr1–O2	82.53(6)

Figure S4. Comparison of the experimental powder X-ray diffractogram measured on polycrystalline powder introduced with their mother solution in capillary tube with the calculated ones of **2**.

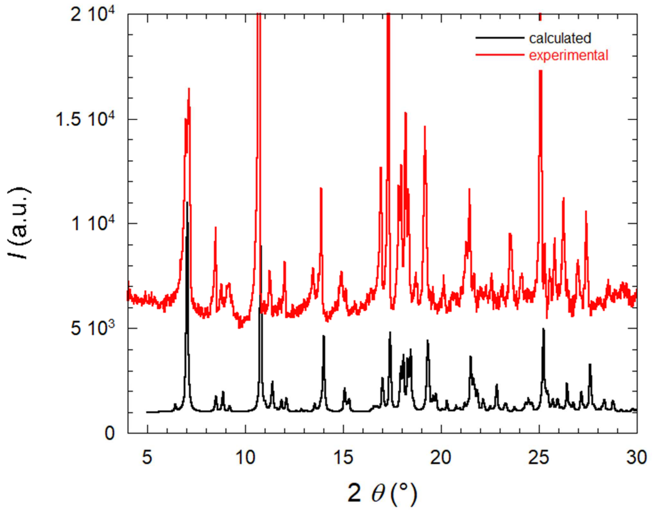

Figure S5. Molecular structure of $[Cr(L)(CN)_2Mn(H_2L^2)][Cr(L)(CN)_2]\cdot5.5H_2O\cdot3MeOH$, **3** showing the asymmetric unit excluding the solvent molecules (a) with thermal ellipsoids fixed at 30 % and (b) in balls and sticks. View of the crystal packing (c) in the (*a*,*c*) and (d) (*a*,*b*) plane. The dashed red line materializes the shortest intermolecular metal-metal distance (indicated in Å). Color scheme: C = grey, H = dark grey, N = blue, O = red, K = blue green, Cr = green and Mn = yellow.

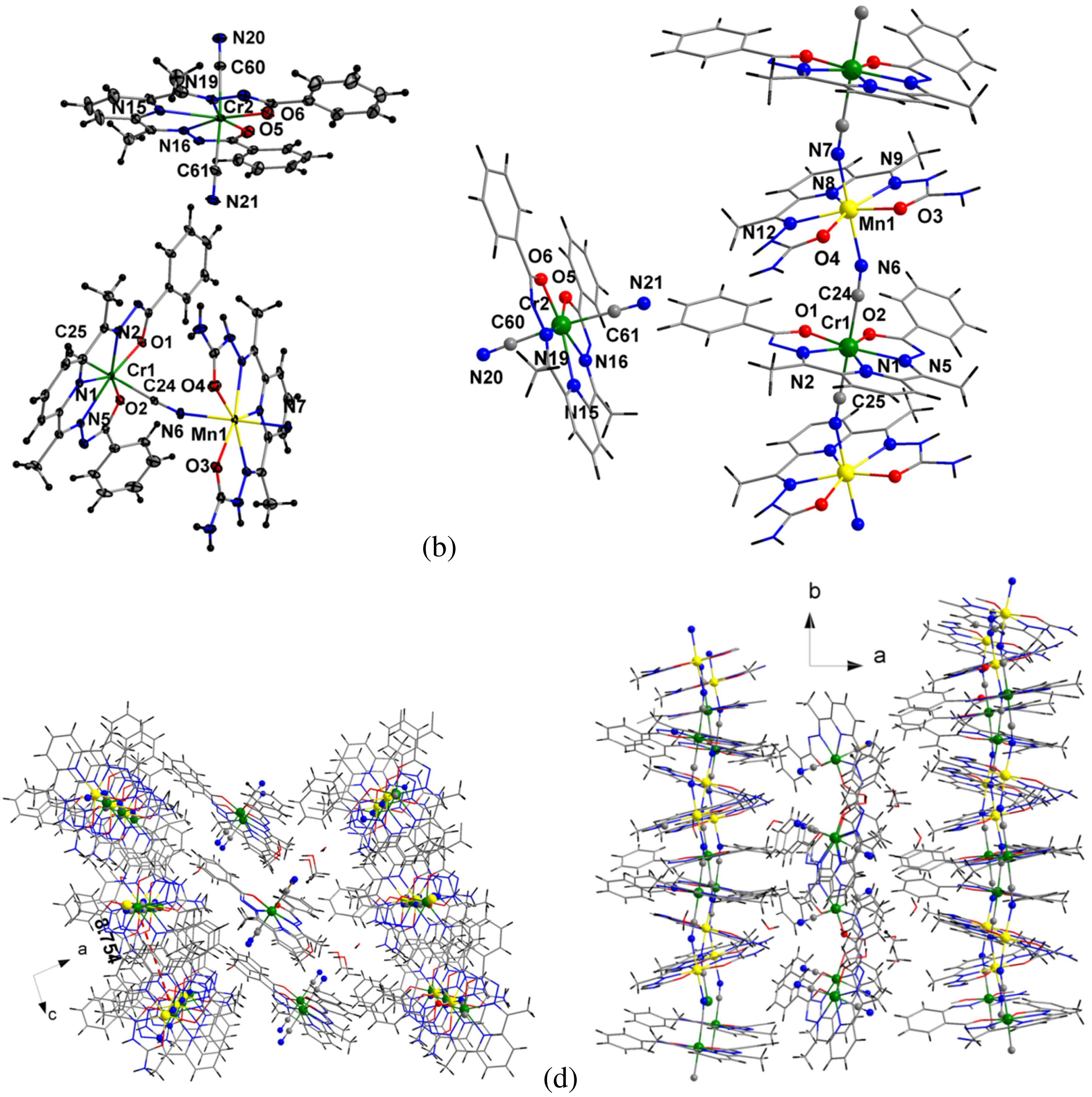

(a) (b)

(c) (d)

Table S6. Selected bond lengths of **3** (Å).

Cr1–C24	2.096(2)	Cr1–C25	2.088(2)	Cr1–N1	2.391(1)
Cr1–N2	2.247(2)	Cr1–N5	2.184(2)	Cr1–O1	1.977(2)
Cr1–O2	1.959(1)	Cr2–C60	2.091(2)	Cr2–C61	2.095(4)
Cr2–N15	2.394(2)	Cr2–N16	2.182(2)	Cr2–N19	2.253(2)
Cr2–O5	1.956(2)	Cr2–O6	1.978(2)	Mn1–N7	2.220(2)
Mn1–N6	2.239(2)	Mn1–N2	2.338(2)	Mn1–N9	2.330(2)
Mn1–N12	2.298(2)	Mn1–O3	2.210(1)	Mn1–O4	2.245(1)

Table S7. Selected bond angles of **3** (°).

C24–Cr1–C25	178.48(7)	C24–Cr1–N1	89.42(6)
C25–Cr1–N1	91.89(6)	C24–Cr1–N2	89.32(6)
C25–Cr1–N2	91.93(7)	N1–Cr1–N2	65.40(6)
C24–Cr1–N5	91.20(6)	C25–Cr1–N5	88.64(6)
N1–Cr1–N5	65.80(6)	N2–Cr1–N5	131.19(6)
C24–Cr1–O1	90.18(6)	C25–Cr1–O1	89.38(6)
N1–Cr1–O1	137.52(6)	N2–Cr1–O1	72.12(6)
N5–Cr1–O1	156.66(6)	C24–Cr1–O2	89.04(6)
C25–Cr1–O2	89.47(6)	N1–Cr1–O2	139.87(6)
N2–Cr1–O2	154.64(6)	N5–Cr1–O2	74.15(6)
O1–Cr1–O2	82.58(5)	C60–Cr2–C61	174.84(9)
C60–Cr2–N15	88.01(7)	C61–Cr2–N15	87.21(8)
C60–Cr2–N16	89.00(7)	C61–Cr2–N16	87.30(7)
N15–Cr2–N16	66.31(6)	C60–Cr2–N19	90.40(7)
C61–Cr2–N19	89.36(8)	N15–Cr2–N19	65.12(6)
N16–Cr2–N19	131.42(6)	C60–Cr2–O5	90.90(7)
C61–Cr2–O5	91.54(8)	N15–Cr2–O5	140.41(6)
N16–Cr2–O5	74.10(6)	N19–Cr2–O5	154.47(6)
C60–Cr2–O6	92.56(7)	C61–Cr2–O6	92.27(8)
N15–Cr2–O6	137.28(6)	N16–Cr2–O6	156.38(6)
N19–Cr2–O6	72.16(6)	O5–Cr2–O6	82.31(6)
N7–Mn1–N6	174.49(6)	N7–Mn1–N8	93.29(6)
N6–Mn1–N8	92.19(6)	N7–Mn1–N9	87.46(6)
N6–Mn1–N9	95.24(6)	N8–Mn1–N9	66.73(6)
N7–Mn1–N12	95.83(6)	N6–Mn1–N12	85.75(6)
N8–Mn1–N12	67.40(6)	N9–Mn1–N12	134.13(6)
N7–Mn1–O3	86.72(6)	N6–Mn1–O3	89.69(6)
N8–Mn1–O3	136.63(6)	N9–Mn1–O3	69.95(6)
N12–Mn1–O3	155.78(6)	N7–Mn1–O4	90.79(6)
N6–Mn1–O4	84.77(6)	N8–Mn1–O4	137.64(6)
N9–Mn1–O4	155.62(5)	N12–Mn1–O4	70.24(6)
O3–Mn1–O4	85.68(5)	Mn1–N6–C24	160.41(1)
Mn1–N7–C25	160.63(2)	Mn1–N6–C24	160.41(16)
Cr1–C24–N6	172.35(2)	Cr1–C25–N7	173.08(2)
Cr2–C60–N20	178.52(2)	Cr2–C61–N21	177.2(2)

Figure S6. Comparison of the experimental powder X-ray diffractogram measured on polycrystalline powder introduced with their mother solution in capillary tube with the calculated ones of **3**.

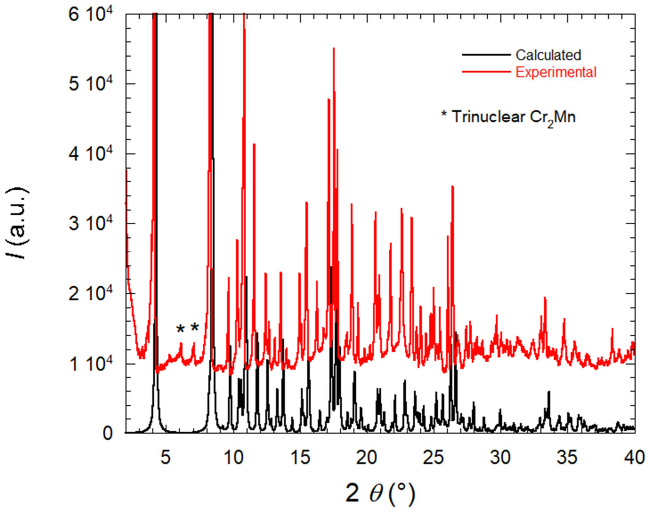

Figure S7. (a) Asymmetric unit of [Cr(L)(CN)$_2$Mn(H$_2$L^3)][Cr(L)(CN)$_2$]·6H$_2$O, **4** with thermal ellipsoids fixed at 30 %. Crystal packing of **4** (b) in the (*a*,*c*) and (c) in the (*b*,*c*) plane. The dashed red lines materialize the shortest intermolecular metal-metal distance (indicated in Å). Color scheme: C = grey, H = dark grey, N = blue, O = red, K = blue green, Cr = green and Mn = yellow.

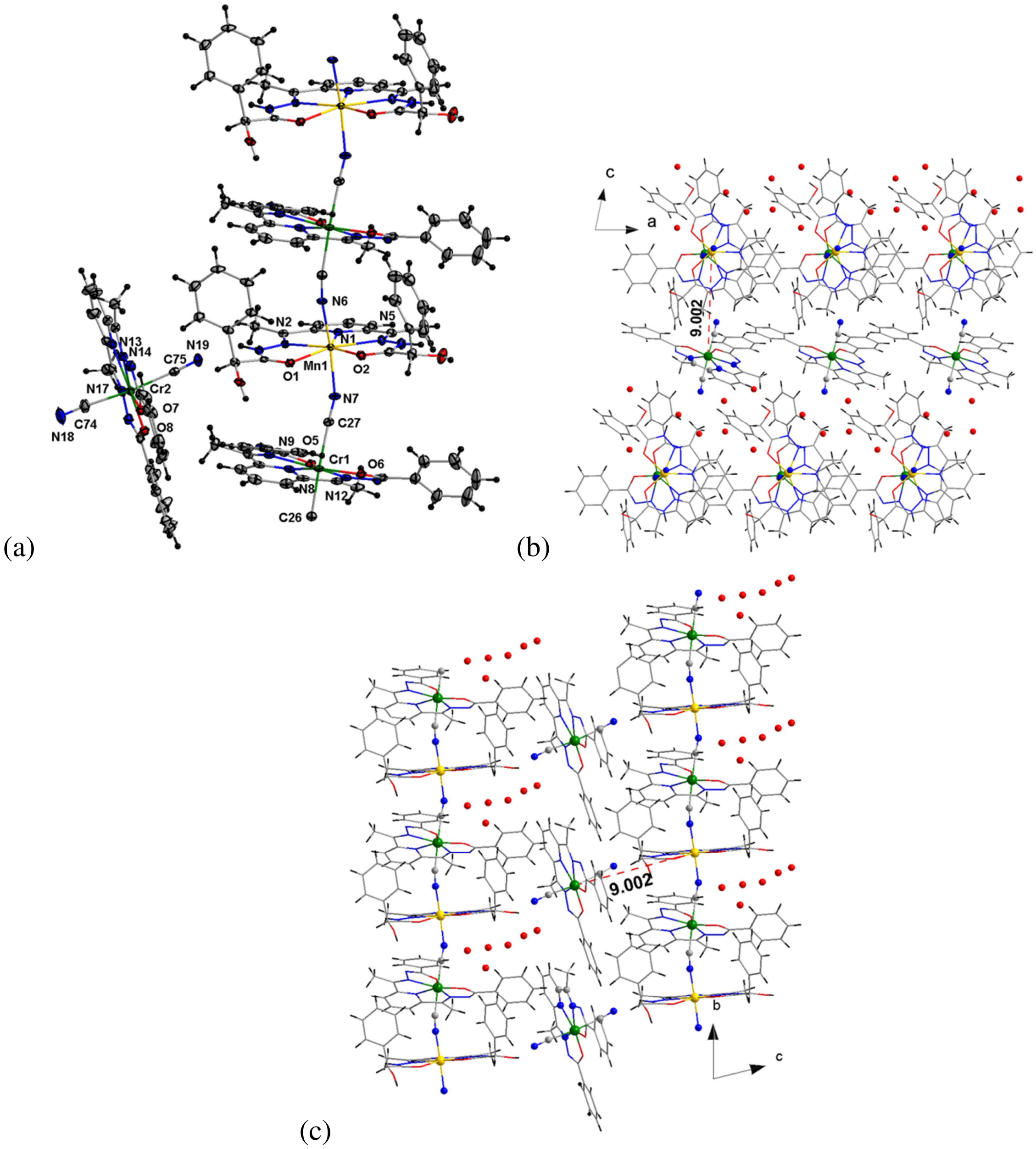

(a)

(b)

(c)

Table S8. Selected bond lengths of **4** (Å).

O1–Mn1	2.278(2)	O2–Mn1	2.346(3)	O5–Cr1	1.975(2)
O6–Cr1	1.960(2)	O7–Cr2	1.952(3)	O8–Cr2	1.968(3)
N1–Mn1	2.335(3)	N2–Mn1	2.321(3)	N5–Mn1	2.300(3)
N6–Mn1	2.178(3)	N7–Mn1	2.189(3)	N8–Cr1	2.397(3)
N9–Cr1	2.246(3)	N12–Cr1	2.179(3)	N13–Cr2	2.363(3)
N14–Cr2	2.184(3)	N17–Cr2	2.244(3)	C74–Cr2	2.089(4)
C75–Cr2	2.094(4)	C26–Cr1	2.096(4)	C27–Cr1	2.080(3)

Table S9. Selected bond angles of **4** (°).

C26–N6–Mn1	164.4(3)	C27–N7–Mn1	157.5(3)
N18–C74–Cr2	173.1(5)	N19–C75–Cr2	173.8(3)
N7–Mn1–N6	166.52(1)	N7–Mn1–O1	81.65(1)
N6–Mn1–O1	86.85(1)	N7–Mn1–N5	90.64(1)
N6–Mn1–N5	97.03(1)	O1–Mn1–N5	155.42(1)
N7–Mn1–N2	92.98(1)	N6–Mn1–N2	89.55(1)
N7–Mn1–N1	96.89(1)	N6–Mn1–N1	96.27(1)
O1–Mn1–N1	136.17(1)	N5–Mn1–N1	67.74(1)
N2–Mn1–N1	66.74(1)	N7–Mn1–O2	85.55(1)
N6–Mn1–O2	86.83(1)	O1–Mn1–O2	86.90(9)
N5–Mn1–O2	69.18(1)	N2–Mn1–O2	156.37(9)
N1–Mn1–O2	136.87(9)	N12–Cr1–N9	130.79(1)
N12–Cr1–C26	83.55(1)	N9–Cr1–C26	96.47(1)
N12–Cr2–C27	88.34(1)	N9–Cr1–C27	87.45(1)
C26–Cr1–C27	171.69(1)	N12–Cr1–N8	66.20(1)
N9–Cr1–N8	64.91(1)	C26–Cr1–N8	83.75(1)
C27–Cr1–N8	91.34(1)	N12–Cr1–O5	156.97(1)
N9–Cr1–O5	72.22(1)	C26–Cr1–O5	95.87(1)
C27–Cr1–O5	92.30(1)	N8–Cr1–O5	136.75(1)
N12–Cr1–O6	74.45(1)	N9–Cr1–O6	154.18(1)
C26–Cr1–O6	91.42(1)	C27–Cr1–O6	88.13(1)
N8–Cr1–O6	140.64(1)	O5–Cr1–O6	82.56(1)
N14–Cr2–N17	132.99(1)	N14–Cr2–C75	84.11(1)
N17–Cr2–C75	94.85(1)	N14–Cr2–C74	92.74(2)
N17–Cr2–C74	83.73(2)	C75–Cr2–C74	174.21(1)
N14–Cr2–N13	67.11(1)	N17–Cr2–N13	65.94(1)
C75–Cr2–N13	86.03(1)	C74–Cr2–N13	88.27(1)
N14–Cr2–O8	154.96(1)	N17–Cr2–O8	72.01(1)
C75–Cr2–O8	93.27(1)	C74–Cr2–O8	91.63(2)
N13–Cr2–O8	137.71(1)	N14–Cr2–O7	73.45(1)
N17–Cr2–O7	153.37(1)	C75–Cr2–O7	90.75(1)
C74–Cr2–O7	93.01(1)	N13–Cr2–O7	140.55(1)
O8–Cr2–O7	81.71(1)		

Figure S8. (a) Solid state circular dichroism and (b) absorption spectra measured on **3**.

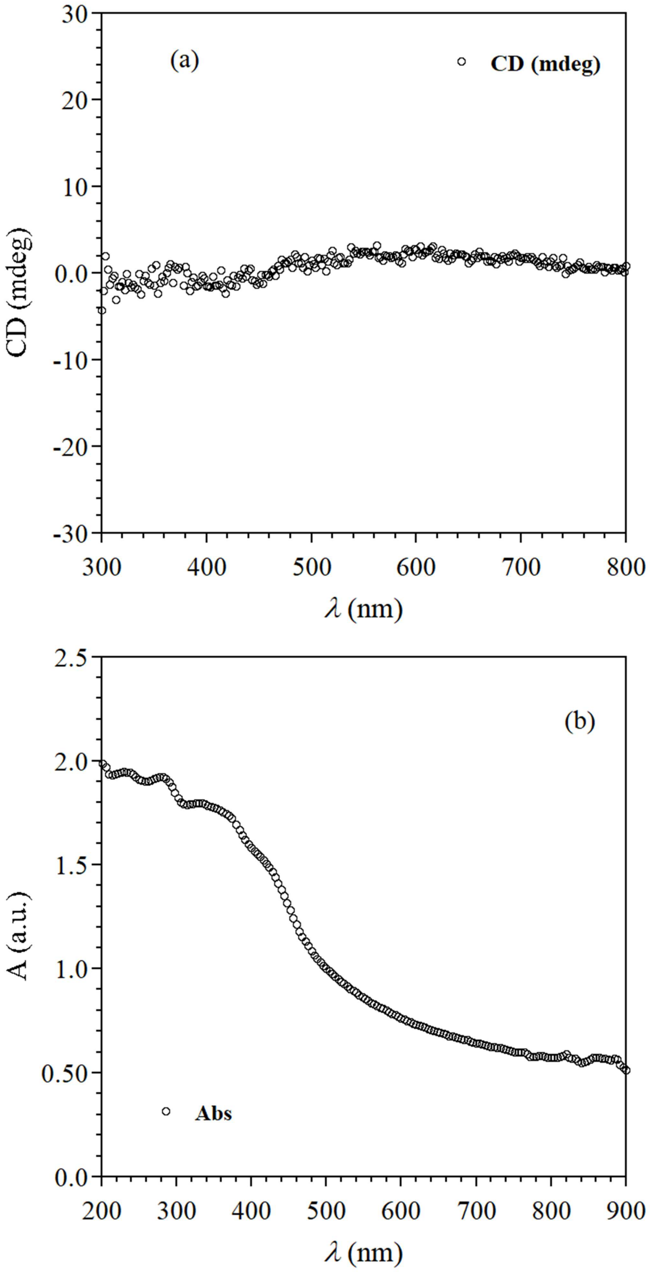

Figure S9. Comparison of the experimental powder X-ray diffractogram measured on polycrystalline powder introduced with their mother solution in capillary tube with the calculated ones of **4**.

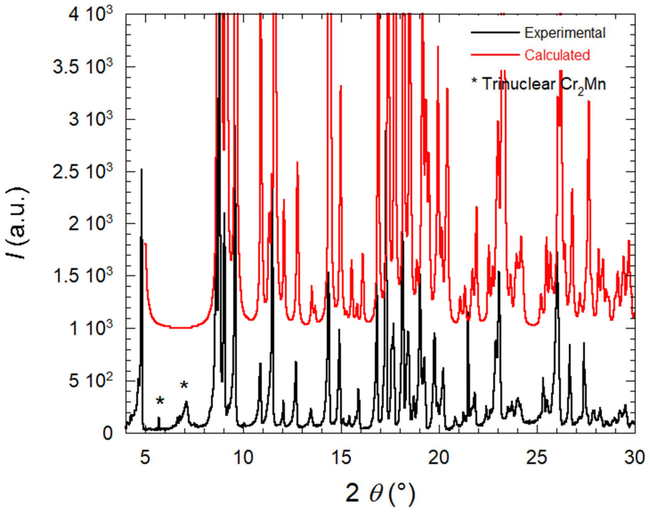

Figure S10. Experimental (O) and calculated (—) temperature dependence of $\chi_M T$ = f(T) curves of **3** and **4**. The best fit parameters are discussed in the text.

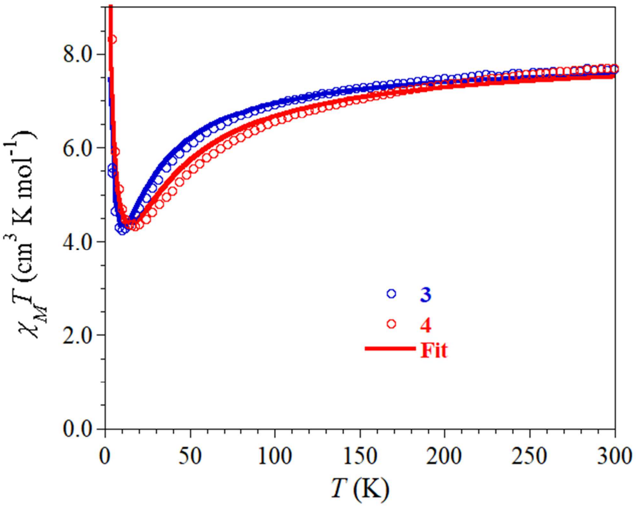

Figure S11. Field dependence of the magnetization measured at 2 K for (a) **1** – **2** and (b) **3** – **4**.

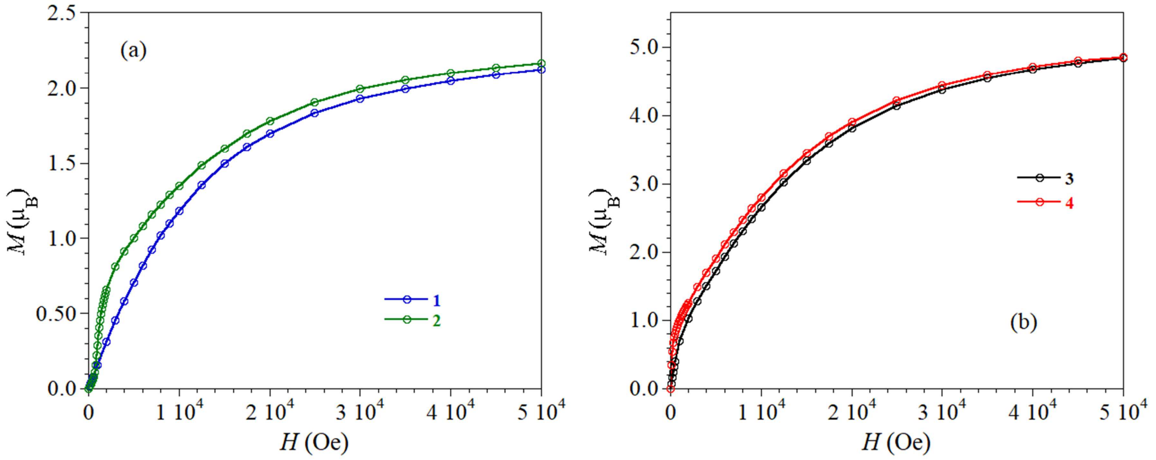

Figure S12. (a) Temperature dependence of the susceptibility χ under applied dc fields of 100 to 4000 Oe and (b) field dependence of the magnetization derivative dM/dH measured between 2 and 8 K for **2**.